Heavy mineral and detrital zircon provenance signatures of sandstones in A05-1 and A15-1, Dutch sector, North Sea

HM Research Associates Report HMRA/21/05

October 2021

for

EBN B.V.
Daalsesingel 1
3511 SV Utrecht
The Netherlands

HM Research Associates
Giddanmu
St Ishmaels
Haverfordwest SA62 3TJ
United Kingdom

Tel: 01646 636592
e-mail: heavyminerals@hotmail.co.uk

INTRODUCTION

This report details the results of a provenance study of probable Triassic sandstones in two wells in Dutch North Sea Quadrant A, commissioned by EBN as part of a prospectivity review of the Early Triassic play in the area. Triassic play concepts include classic models of fluvial sediment input into the Southern Permian Basin from source areas located south of the basin, with aeolian reworking by northeastern tradewinds. The current project area is located at the northern edge of the Southern Permian Basin, and in this provenance model, reservoir sand deposition depends on long-distance fluvial and aeolian transport with preferential fining of sediment from south to north (Ziegler, 1990; Doornenbal and Stevenson, 2010). This model therefore poses critical risks to both reservoir presence and effectiveness in the Triassic of Quadrant A.

However, an alternative play concept is the introduction of northerly sourced clastic sediments, in combination with the creation of local accommodation space due to syn-sedimentary tectonic activity related to salt movement. This hypothetical play concept would improve the chance of success for both reservoir presence and effectiveness, and therefore prospectivity. Analogue conditions to such a hypothetical model are found onshore Denmark, where heavy mineral compositions and zircon geochronology have provided indications for sediment sourcing from the northerly located Baltic Shield (Olivarius et al., 2015).

A pilot heavy mineral and zircon geochronology study was initiated in order to help assess which provenance model is more likely. The study involved two wells, A05-1 and A15-1 (Fig. 1).

The A05-1 well (Amerada Hess) encountered an interval between ~ 3125-3185 m AHRT (60 m thickness) consisting of alternating mudstones and sandstones with unclear geological age (ranging from Lower Triassic to Late Jurassic) and origin (Kerstholt-Boegehold and Munsterman, 2016). Sediments in the interval were attributed to the Lower Triassic by Amerada Hess (2000), although there are no clear diagnostic criteria to support this statement. The report by Amerada Hess (2000) refers to unpublished data from the German B/4-2 well that could be relevant: *Middle Bunter sandstones were penetrated in well B/4-2 and are of excellent reservoir quality. The sands represent deposition from ephemeral river systems depositing sediments transported by sheetfloods into basinal locations. A Triassic event was mapped within the prospect area and the possibility of encountering Triassic sandstones is acknowledged*. This appears to provide information that a north-south oriented fluvial system was indeed present, feeding sediment into the Southern Permian Basin,

possibly linking up with (Triassic?) fluvial feeder systems penetrated in the Danish Bertel-1 well further to the north.

The A15-1 well (Placid) was drilled ~ 40 km southeast of the A05-1 well and encountered Triassic deposits between ~ 2530-3342 m AHRT (ca 750m thickness) varying in age from Norian (Keuper) at the top to Induan (Lower Buntsandstein) at the base. The lithostratigraphic classification of this well more or less follows the classical German tri-partite applied in the Dutch lithostratigraphic nomenclature (Adrichem Boogaert and Kouwe, 1993), and deposits classified as Volpriehausen and Detfurth Formations can be correlated confidently to the Dutch type sections further south. This well therefore could act as a robust and most northwards located reference section indicative for influx of sediment from the south or southeast.

HEAVY MINERAL ANALYSIS: PRINCIPLES

Heavy mineral assemblages are sensitive indicators of sediment provenance. A large number of species have been found in sandstones, many of which have restricted parageneses that provide a positive indication of the mineralogical composition of the source region. Differences in heavy mineral assemblages facilitate the discrimination of sand bodies derived from different sources via different sediment transport pathways. Stratigraphic changes in heavy mineral assemblages provide a basis for correlation, independent of traditional biostratigraphic or log correlation methods.

Controls on heavy mineral assemblage compositions

Although source rock mineralogy is the ultimate control on heavy mineral assemblage composition, several other processes operative during the sedimentary cycle may overprint the original provenance signal. These processes can introduce a large degree of heterogeneity to assemblages that were derived from the same source and were therefore originally homogeneous. It is crucial for accurate provenance and correlation studies that these factors are fully appreciated and accounted for. The processes are:

Weathering: this process causes modification of source rock mineralogy both at source (prior to incorporation into the transport system) and during periods of exposure on the floodplain during transport (alluvial storage).

Abrasion: this process may reduce proportions of mechanically unstable minerals. Mechanically-induced depletion of minerals may occur through abrasion during transport.

Assemblages recovered from ditch cuttings samples may also be affected by abrasion through the aggressive action of the drill bit.

Hydraulic processes: variations in hydrodynamic conditions during transport and deposition strongly affect relative abundances of minerals with different hydraulic behaviour (controlled by grain size, density and shape).

Diagenesis: this process selectively removes unstable minerals during burial diagenesis through the action of elevated temperature pore waters.

Source rock mineralogy is undoubtedly altered during weathering process, but the extent to which this affects the detrital mineralogy has not been comprehensively evaluated. However, qualitative studies of modern river sediments indicate that there is little or no actual reduction in mineral diversity between source rock and transport system. Furthermore, the extent of source-area weathering can be justifiably viewed as a provenance-related feature that might have potential value in correlation studies (for example, in sequences deposited during periods of climate change).

Abrasion during transport is rarely an important factor in controlling heavy mineral assemblages. Although experimental work has shown that some loss of minerals does occur with prolonged simulated transport, case studies have failed to demonstrate that it occurs to any appreciable extent in natural systems. By contrast, there is evidence that minerals may be depleted through the action of the drill bit, as core and cuttings samples over equivalent sections commonly have slightly different mineralogical compositions. The most severely affected mineral appears to be apatite, presumably because of its relatively low hardness.

The processes of weathering on the floodplain during periods of exposure, and of weathering at the site of deposition, are potentially significant factors, as are variations in hydraulic conditions during deposition and in the extent of burial diagenesis. Both weathering and burial diagenesis reduce detrital mineral diversity through dissolution of unstable species. The effects of burial diagenesis are particularly significant and pervasive, being marked by a clear and well-defined progressive reduction in mineral diversity with depth. This is essentially caused by increased dissolution rates resulting from the higher pore fluid temperatures that occur with increasing depth. The relative stability of heavy minerals under both deep burial and weathering are relatively well known, the most significant difference between the two processes being that apatite is unstable during weathering but stable in deep burial. Thus, absence or reduced contents of apatite suggest that acidic groundwaters may have influenced heavy mineral suites.

Variations in hydraulic conditions during deposition modify the relative proportions of minerals with different hydraulic behaviour. The principal factors influencing hydraulic behaviour are grain size and density. Therefore, changes in hydraulic conditions cause variations in the ratio of denser minerals, such as zircon, garnet or rutile, to the less dense minerals, such as apatite and tourmaline. Grain shape also influences hydraulic behaviour, but this is generally a less important factor, the most obvious exception to this statement being mica, which, although having the density of a heavy mineral, actually behaves as a light mineral.

For detailed discussion of the effects of all the factors described above, see Morton (2012).

Provenance-sensitive parameters

In order to accurately reconstruct provenance and generate correlation frameworks, the effects of weathering, diagenesis and depositional processes must be minimised. This can be achieved in two ways.

The first approach is to utilise the conventional heavy mineral data (data acquired by petrographic analysis of the mineral assemblages). Identification of variations in sediment source from the conventional data is best made by determining ratios of stable minerals with similar densities, as these are not affected by changes in hydraulic conditions during sedimentation or by diagenetic processes (Morton and Hallsworth, 1994). Ratios that best reflect provenance characteristics are apatite:tourmaline (ATi), garnet:zircon (GZi), rutile:zircon (RuZi), monazite:zircon (MZi) and chrome spinel:zircon (CZi). In some circumstances, ATi and GZi may not provide a true reflection of the source composition. For example, ATi may be reduced during weathering, and GZi may be lowered during burial diagenesis.

The alternative approach to identifying changes in provenance is to undertake varietal studies. These are studies that concentrate on variations seen within one mineral group, thereby strongly diminishing the range of density and stability within the data set. The classical approach to varietal studies is to distinguish types on the basis of their optical properties, such as crystal form or colour, but this approach is commonly subjective and class distinctions tend to be somewhat arbitrary. However, this approach may provide useful information on sedimentary processes (for example, using the extent to which grains are rounded). A more objective approach is to determine the geochemical characteristics of a mineral population (mineral chemical analysis). Methods that are widely used include

determination of major element compositions by electron microprobe analysis (EMPA), trace element compositions by laser ablation inductively coupled plasma-mass spectrometry (LA-ICP-MS), and single grain age dating by sensitive high-resolution ion microprobe (SHRIMP) or laser ablation sector field inductively coupled plasma-mass spectrometry (LA-SF-ICP-MS). Mineral chemical analysis also has the advantage of generating data sets that can be readily compared with those generated by other analysts. In this study, varietal analysis concentrated on determination of apatite roundness, since this proved crucial in studies in the UK Central North Sea Triassic (Mouritzen et al., 2017). In addition, zircons from one sample in A15-1 were dated by U-Pb to establish whether northerly or southerly sources are more likely.

HEAVY MINERAL ANALYSIS: METHODS

Sample preparation

The cuttings samples were cleaned using detergent and a Soniprep ultrasonic probe to remove and disperse any clay that might have been adhering to grain surfaces, washed through a 63 μm sieve and resubjected to ultrasonic treatment until no more clay passed into suspension, and wet sieved through the 125 and 63 μm sieves, The resulting >125 μm and 63-125 μm fractions were dried in an oven at 80^{o}C and the 63-125 μm fractions were placed in bromoform with a measured specific gravity of 2.8. Heavy minerals were allowed to separate under gravity, with frequent stirring to ensure complete separation. The heavy mineral separates were mounted under Canada Balsam for optical study using a polarising microscope, with a split being retained for additional work where recovery allowed.

Conventional analysis and ratio determination

Three types of data were acquired from the heavy mineral separates. Initially, the relative abundance of non-opaque heavy minerals and other components of the separates (such as barite, diagenetic minerals, opaques and mica) were estimated on the basis of a 200 grain count (Table 1). Proportions of non-opaque detrital heavy minerals (Table 2) were estimated by counting 200 non-opaque detrital grains using the ribbon method described by Galehouse (1971), where grain recovery allowed. Identification was made on the basis of optical properties, as described for grain mounts by Mange and Maurer (1992). Provenance-sensitive mineral indices (Morton and Hallsworth, 1994) were also determined using the ribbon counting method, ideally on the basis of a 100-200 grain count (Table 3). Apatite roundness indices (ARi) were determined using the criteria discussed by Morton et al. (2010). It was not

always possible to achieve the optimum grain count for the indices because of the scarcity of some of the mineral phases.

Zircon geochronology

Zircon grains were extracted from the heavy mineral fraction of one sample from A15-1 using an optical microscope, mounted on double-sided, transparent adhesive tape and subsequently embedded in 1-inch diameter circular epoxy mounts for polishing. In order to study their internal structure, backscatter electron (BSE) images of all analysed zircons were obtained using a Philips XL 40 scanning electron microscope.

U-Pb age data were obtained at the Central Analytical Facility, Stellenbosch University, by laser ablation - single collector - magnetic sectorfield - inductively coupled plasma - mass spectrometry (LA-SF-ICP-MS) employing a Thermo Finnigan Element2 mass spectrometer coupled to a NewWave UP213 laser ablation system. All age data presented here were obtained by single spot analyses with a spot diameter of 30 μm and a crater depth of approximately 15-20 μm, corresponding to an ablated zircon mass of approximately 150-200 ng. The methods employed for analysis and data processing are described in detail by Gerdes and Zeh (2006) and Frei and Gerdes (2009). For quality control, the Plešovice (Sláma et al. 2008) and M127 (Mattinson, 2010; Nasdala et al., 2008) zircon reference materials were analysed, and the results were consistently in excellent agreement with the published ID-TIMS ages. Full analytical details and the results for all quality control materials analysed are reported in Table 4. The calculation of concordia ages and plotting of concordia diagrams were performed using Isoplot/Ex 3.0 (Ludwig, 2003). Stacked histogram – relative probability plots of the zircon age populations were plotted using AgeDisplay (Sircombe, 2004).

HEAVY MINERAL ASSEMBLAGES

All samples yielded large heavy mineral separates despite the small sample sizes, but detrital non-opaque minerals form only a small proportion of the heavy mineral separates (mostly <0.5% with a maximum of 2%).

Well A05-01

Separates from A05-01 are flooded with barite (Table 1, Fig. 2), and consequently detrital minerals are proportionally scarce owing to the super-abundance of this drilling additive mineral. Analysis of the first mounts prepared from the 13 analysed samples yielded between

7 and 118 detrital grains. Data quality was improved by analysing an extra two slides for each sample, and consequently heavy mineral % data are now based on between 28 to 200 grains (Table 2). The variations in detrital mineral abundance are likely to be controlled by lithology, since the succession comprises interbedded sandstones and mudstones, the latter being unproductive for heavy minerals owing to grain size. Owing to the combination of barite contamination and variable lithology, provenance-sensitive index values tend to be based on low counts (Table 3) and in a small number of cases, data used in the plots have been pooled from adjacent samples.

Detrital assemblages (Table 2, Fig. 3) are dominated by diagenetically-stable minerals (mean contents of 38% apatite, 5% rutile, 16% tourmaline and 27% zircon), with garnet also common (mean 6%). The garnet grains are highly corroded and original proportions are likely to be been significantly higher. Accordingly, garnet:zircon (GZi) values are not representative of provenance characteristics.

A large proportion of apatite grains are well-rounded, with apatite roundness indices (ARi) between 25 and 61. There is a distinct fall in ARi values towards the top of the succession, with the samples from 3124-3143 m having values ~ 25-30, whereas the majority lower in the unit have values ~ 50-60 (Fig. 4).

Provenance-sensitive index values show comparatively little variation through the analysed interval (Table 3, Fig. 4). ATi (apatite:tourmaline index) shows the most heterogeneity, with values between 56 and 88. Other parameters are consistently low, with rutile:zircon index (RuZi) between 10 and 23: monazite:zircon index (MZi) and chrome spinel:zircon undex (CZi) are zero throughout.

The hydrodynamically-controlled index zircon:apatite (ZAi) shows major variations (14-65), reflecting differences in grain size. The lower part of the succession (below 3146 m) has relatively uniform ZAi, but the upper part is more variable. These patterns suggest there is little variation in grain size in the lower part of the well but greater heterogeneity in the upper part. This change corresponds to the observed fall in ARi and may indicate a subtle difference in provenance.

Well A15-01

Separates from A15-01 are rich in carbonate particles, mostly as fine-grained aggregates probably derived from interbedded mudstones. Barite is much less abundant than in A05-01 (Table 1, Fig. 2). Detrital minerals are slightly more common than in A05-01, ranging from 8

to >200 grains present on the mounts prepared from the 13 analysed samples (Table 2). As with A05-01, the variations in detrital mineral abundance are likely to be controlled by lithology.

Detrital assemblages (Table 2, Fig. 3) are dominated by diagenetically-stable minerals (mean contents of 48% apatite, 2% rutile, 13% tourmaline and 30% zircon), with garnet also common (mean 5%). The garnet grains are highly corroded and original proportions are likely to be been significantly higher. Accordingly, GZi values are not considered to be representative of provenance characteristics.

A large proportion of apatite grains are well-rounded (Table 3, Fig. 5), with apatite roundness indices (ARi) between 46 and 64.

Apatite:tourmaline index values (ATi) show little variation through the Triassic succession, with values between 62 and 92. Other provenance-sensitive parameters cannot be accurately determined for individual samples owing to low counts. However, combining data across the entire succession shows that RuZi is low (4.2).

The hydrodynamically-controlled index zircon:apatite (ZAi) shows major variations (6-64), reflecting differences in grain size. ZAi is highest towards the base of the succession and lowest at the top, suggesting the succession has an overall upward-fining profile.

Comparison of A05-01 and A15-01

Detrital heavy mineral assemblage compositions are closely comparable in the two wells suggesting they have a common provenance and are potentially correlatable. ATi and ARi are the most useful high-resolution parameters for comparison between the two successions, since apatite is the most abundant mineral and the rounded morphology is distinctive. The ATi-ARi crossplot (Fig. 6) shows that the two successions have partly overlapping characteristics, confirming the conventional heavy mineral assemblage evidence for a common provenance. However, it is likely that the upper part of the succession in A05-01 (3124-3130 m) does not correlate with any of the succession in A15-01, since it has lower ARi values that do not match those in A15-01. The abundance of well-rounded apatite suggests that the Triassic sandstones in the two wells have undergone significant aeolian transport. This may have taken place during the Triassic depositional cycle, but alternatively could indicate recycling from a precursor aeolian succession (such as the Rotliegendes).

Regional comparisons

Heavy mineral characteristics of the Skagerrak succession in well 22/24b-5Z, UK central North Sea (Mouritzen et al., 2017), are compared with A05-01 and A15-01 using the ATi-ARi plot. The data demonstrate the existence of marked differences between the two areas, with UK Quadrant 22 sandstones having consistently lower ARi values and generally higher ATi values.

The greatest difference is shown by the younger Joanne sandstones (Ladinian-Carnian), which have very high ATi and low ARi. The underlying Judy (Anisian-Ladinian) and the oldest Smith Bank and Marnock Mudstone intervals (Induan-Olekinian) have a higher proportion of well-rounded apatite and slightly lower ATi values. Although there is no overlap between the characteristics shown by the UK Quadrant 22 sandstones and the Dutch northern offshore area, the closest similarity is with the Judy-Smith Bank interval.

Further evidence for differences between these two areas is given by rutile:zircon index (RuZi) data. RuZi is low in Dutch Quadrant A (4.2-13.5), whereas mean values in the Joanne, Judy and Smith Bank sandstones are much higher (34.3, 29.1 and 32.1 respectively).

Heavy mineral data are available from the Volpriehausen and Solling Members (Bunter Sandstone Formation) in the northern part of the North German Basin. Non-opaque heavy mineral assemblages are markedly different to those in Dutch Quadrant A, with garnet being considerably more abundant (Olivarius et al., 2015). However, this difference cannot be ascribed to provenance variations, since burial-related diagenesis has led to extensive garnet depletion in the A05-01 and A15-01 wells. Further comparison is not possible owing to the difference in analytical methods employed in the current study compared with Olivarius et al. (2015), who analysed the entire grain size range by computer-controlled scanning electron microscopy (CCSEM). However, the Volpriehausen Member in the North German Basin includes aeolian sediment derived from the Variscan Belt to the south (Olivarius et al., 2015). Given the abundance of well-rounded apatite in the Triassic in Dutch Quadrant A, it is therefore possible that Variscan-sourced sediment reached the Dutch northern offshore area.

ZIRCON GEOCHRONOLOGY

The study of the Bunter Sandstone Formation in the northern part of the North German Basin by Olivarius et al. (2015) showed that zircon ages are distinctly different between the aeolian Volpriehausen Member and the fluvial Solling Member. The Volpriehausen Member was derived from the south on the basis of abundant Variscan-age zircons, whereas the Solling

Member was derived from the Ringkøbing-Fyn High to the north on the basis of a marked reduction in the Variscan component in conjunction with an influx of mid-Proterozoic zircons. Zircon age data are also available from the UK Central North Sea Triassic (Greig, 2021), which is believed to be sourced from a combination of Scotland and Scandinavia (McKie, 2014).

In view of the diagnostic information likely to be gained from zircon age data, zircons were mounted from A15-1 for U-Pb analysis. It was not possible to analyse zircons from A05-1 owing to the extensive barite contamination, but by combining separates for the samples in the 9770-9820 ft interval, sufficient zircons were available for the study. Given the uniformity in heavy mineral provenance data, combining ditch cuttings samples is considered a valid approach although inevitably the spectrum acquired will give a composite picture of the succession. The full analytical dataset is given in Table 5.

The majority of zircon grains yielded concordant or near-concordant U-Pb isotopic compositions, as demonstrated by their proximity of the concordia curve on Wetherill plots (Fig. 7). Of the 114 analysed grains, 105 are < 10% discordance, and the remaining 9 yield ages that are consistent with the concordant analyses (Fig. 8).

The great majority of the zircons yield Meso- and Palaeoproterozoic ages (Fig. 8), with a large peak at 1000-1300 Ma, with three subsidiary peaks at c. 1500 Ma, 1650 Ma and 1800 Ma. In addition, there is a small number of Archaean and late Neoproterozoic-Phanerozoic zircons (Fig. 8). Most of the Phanerozoic ages are in the 400-500 Ma range, but there are five younger zircons, two dated as c. 291 Ma and three between c. 340 Ma and 344 Ma.

The zircon age spectrum from A15-1 is compared with those acquired from the Volpriehausen and Solling members by Olivarius et al. (2015) in Fig. 9. There is a marked contrast with the Volpriehausen Member, which has abundant Carboniferous zircons derived from the Variscan belt to the south. There are only five zircons (4.8% of the concordant population) in the A15-1 sample that could have a Variscan source. The spectrum is more akin to those found in the Solling Member, since both are dominated by Meso- and Palaeoproterozoic zircons, indicative of an ultimate Baltican provenance. However, there are distinct differences in the distribution of Proterozoic zircons in the A15-1 sample compared with the North German Basin. The largest group in A15-1 is c. 1000-1300 Ma, corresponding to the Sveconorwegian orogenic event, but this is comparatively minor in the Solling Member.

Detrital zircon data from the Triassic of the Marnock Field, UK Central North Sea, are compared with A15-1 in Fig. 10. There are distinct changes between the three Marnock samples (Joanne, Judy and Smith Bank units). The Joanne sample has more 400-500 Ma zircons (corresponding to the Caledonian orogenic cycle) than Judy and Smith Bank. Also, there is a clear upward increase in abundance of 1550-1700 Ma zircons. At the same time, there is a marked upward decrease in Archaean zircons. The abundance of 900-1350 Ma (Sveconorwegian) and 1350-1550 Ma zircons remains reasonably consistent. The youngest zircons in the Joanne sample are of Caledonian age but the Judy and Smith Bank samples both have younger grains that could be of Variscan origin.

There are some clear similarities with the A15-1 zircons. In particular, the abundance of post-Caledonian zircons is similar to the Smith Bank and, to a lesser extent, the Judy samples. Also, proportions of the 400-500 Ma, 1350-1550 Ma, 1550-1700 Ma and 1700-2000 Ma groups are similar to Smith Bank. The main difference is the abundance of Archaean zircons, which are abundant in Smith Bank and relatively scarce in A15-1.

The zircon data therefore indicate a degree of commonality between A15-1 and the Smith Bank and, to a lesser degree Judy, in the Marnock Field. This is also suggested by the proximity of the A15-1 and A05-1 data to the Smith Bank and Judy data on the ATi-ARi plot (Fig. 6). The increase in Archaean zircons to the north is predictable given the presence of exposed Archaean in the far northwest of Scotland (and by the presence of recycled Archaean zircon in some parts of the Dalradian metasedimentary succession in the Grampian Highlands). The Joanne sandstones, by contrast, are markedly different in terms of apatite morphology and in most aspects in terms of zircon ages (the only similarity being the scarcity of the Archaean component). On this basis, it would appear that the Triassic in the A15 area is equivalent to the older parts of the UK central North Sea Triassic, probably Induan-Olekinian (=Smith Bank), or less likely Anisian (=Judy).

It is possible that some of the zircons in A15-01 were derived from the Ringkøbing-Fyn High, which is believed to have supplied the majority of the zircons in the Solling Member (Olivarius et al., 2015). There is some commonality between the Solling Member and A15-01 spectra, with both areas having peaks at c. 1500 Ma and c. 1650 Ma, and to a lesser extent the older Proterozoic. Late Carboniferous Ketch Fm sandstones in the Southern North Sea have broadly similar zircon spectra to the Solling Member (Fig. 9), being dominated by older Proterozoic zircons (> 1300 Ma), consistent with the interpretation that both were derived from the Ringkøbing-Fyn High (Morton et al., 2001; Morton et al., 2005; Olivarius et al., 2015). There is also a similarity in heavy mineral assemblages since the Ketch Fm is characterised by common chrome spinel, as is the Solling Member in Rødby-1.

CONCLUSIONS

- Heavy mineral data indicate the Triassic sandstones in A05-01 and A15-01 have similar provenance and could therefore be correlatable, although the top part of A05-01 appears slightly different.

- There is a marked difference in heavy mineral parameters between the Joanne sandstones in UK Quadrant 22 and the Triassic in Dutch Quadrant A, indicating they have different provenances. There is a closer similarity between the Triassic in Dutch Quadrant A with the older Judy and Smith Bank Formations in the UK Central North Sea.

- Zircon ages in A15-1 are also similar, but not identical, to those found in the Judy and Smith Bank sandstones in the UK sector.

- The abundance of well-rounded apatite in the Triassic of Dutch Quadrant A indicates either that aeolian processes were important in the deposition of the succession, or that the detritus was recycled from pre-existing aeolian sandstones.

- The Volpriehausen Member in the North German Basin includes aeolian sediment derived from the Variscan Belt to the south. However, despite the likely similarity in terms of apatite roundness, zircon data indicate that the Triassic in A05-1 and A15-1 was unlikely to contain a significant amount of sediment derived from the south.

- Zircon data indicate that the Triassic in A15-1 (and by analogy, A05-1) was mostly derived from Baltican sources. Some input from the Ringkøbing-Fyn High is possible, but the sandstones contain a large group of zircons corresponding to the Sveconorwegian orogeny. Evidence from the North German Basin Triassic and the Carboniferous in the UK Southern Sea indicates that the Ringkøbing-Fyn High is not a major supplier of such zircons, and a more distal origin appears likely.

- The pilot study indicates that north to south sourcing was prevalent in the Triassic of the northern Dutch offshore. It is recommended that further work is undertaken to establish the extent of this transport system and to identify where southerly-derived sediment becomes dominant. Key wells are Bertel-1 in the Danish sector and B/4-2 in the German sector, plus wells in the UK sector such as 43/13-1 and 52/5-1X.

REFERENCES

Adrichem Boogaert van, H. and Kouwe, W., 1993. Stratigraphic nomenclature of the Netherlands, 50. Rijks Geologische Dienst.

Amerada Hess, 2000. Final Geological/Geophysical Report well A/5-1 Dutch Quadrant. Amerada Hess.

Doornenbal, H. and Stevenson, A. (eds.), 2010. Petroleum Geological Atlas of the Southern Permian Basin Area. EAGE Publications, Houten.

Frei, D. and Gerdes, A., 2009. Precise and accurate in situ U–Pb dating of zircon with high sample throughput by automated LA-SF-ICPMS. Chemical Geology, 261, 261-270.

Galehouse, J.S., 1971. Point-counting. In: Carver R.E. (ed.), Procedures in Sedimentary Petrology. Wiley-Interscience, New York, 385-407.

Gerdes, A and Zeh, A., 2006. Combined U–Pb and Hf isotope LA-(MC)-ICP-MS analyses of detrital zircons: comparison with SHRIMP and new constraints for the provenance and age of an Armorican metasediment in Central Germany. Earth and Planetary Science Letters, 249, 47-61.

Greig, I.P., 2021. Heavy mineral stratigraphy and provenance of Triassic sediments of the Central North Sea and Moray Firth. Thesis submitted for PhD, University of Aberdeen, UK.

Jackson, S., Pearson, N., Griffin, W. and Belousova, E., 2004. The application of laser ablation – inductively coupled plasma – mass spectrometry to in situ U-Pb zircon geochronology. Chemical Geology 211, 47-69.

Kerstholt-Boegehold, S. and Munsterman, D., 2016. Jurassic or Triassic? Palynological dating of well A05-01, interval 10250 -10720 ft. TNO Earth, Life & Social Sciences, Utrecht.

Ludwig, K., 2003. Isoplot/Ex version 3: a Geochronological toolkit for Microsoft Excel. Geochronology Center, Berkeley.

Mange, M.A. and Maurer, H.F.W., 1992. Heavy minerals in colour. Chapman and Hall, London.

Mattinson, J.M., 2010. Analysis of the relative decay constants of ^{235}U and ^{238}U by multi-step CA-TIMS measurements of closed-system natural zircon samples. Chemical Geology, 275, 186-198.

McKie, T., 2014. Climatic and tectonic controls on Triassic dryland terminal fluvial system architecture, central North Sea International Association of Sedimentologists, Special Publication, 46, 19-58.

Morton, A.C., 2012. Value of heavy minerals in sediments and sedimentary rocks for provenance, transport history and stratigraphic correlation. In: Sylvester, P. (ed.),

Quantitative Mineralogy and Microanalysis of Sediments and Sedimentary Rocks. Mineralogical Association of Canada Short Course Series, 42, 133-165.

Morton, A.C. and Hallsworth, C.R., 1994. Identifying provenance-specific features of detrital heavy mineral assemblages in sandstones. Sedimentary Geology, 90, 241-256.

Morton, A.C., Hallsworth, C.R. and Claoué-Long J.C., 2001. Zircon age and heavy mineral constraints on provenance of North Sea Carboniferous sandstones. Marine and Petroleum Geology, 18, 319-337.

Morton, A.C., Hallsworth, C.R. and Moscariello, A., 2005. Interplay between northern and southern sediment sources during Westphalian deposition in the Silverpit Basin, southern North Sea. In: Collinson, J.D., Evans, D.J., Holliday, D.S. and Jones, N.S. (eds), Carboniferous hydrocarbon geology: the southern North Sea and surrounding onshore areas. Yorkshire Geological Society Occasional Publication, 7, 135-146.

Morton, A.C., Hallsworth, C.R., Kunka, J., Laws, E, Payne, S. and Walder, D., 2010. Heavy mineral stratigraphy of the Clair Group (Devonian) in the Clair Field, west of Shetland, UK. In: Ratcliffe, K.T. and Zaitlin, B.A. (eds), Application of Modern Stratigraphic Techniques: Theory and Case Histories. SEPM Special Publication, 94, 183-199.

Mouritzen, C., Farris, M.A., Morton, A. and Matthews, S., 2017. Integrated Triassic stratigraphy of the greater Culzean area, UK central North Sea. Petroleum Geoscience, 24, 197-207.

Nasdala, L., Hofmeister, W., Norberg, N., Mattinson, J.M., Corfu, F., Dörr, W., Kamo, S.L., Kennedy, A.K., Kronz, A., Reiners, P.W., Frei, D., Košler, J., Wan, Y., Götze, J., Häger, T., Kröner, A. and Valley, J.W., 2008. Zircon M257 – a homogeneous natural reference material for the ion microprobe U-Pb analysis of zircon. Geostandards and Geoanalytical Research, 32, 247-265.

Olivarius, M., Weibel, R., Friis, H., Boldreel, L., Keulen, N. and Thomsen, T., 2015. Provenance of the Lower Triassic Bunter Sandstone Formation: implications for distribution and architecture of aeolian vs. fluvial reservoirs in the North German Basin. Basin Research, 29, 113-130.

Sircombe, K.N., 2004. AgeDisplay: an EXCEL workbook to evaluate and display univariate geochronological data using binned frequency histograms and probability density distributions. Computers & Geosciences, 30, 21-31.

Sláma, J., Košler, J., Condon, D.J., Crowley, J.L., Gerdes, A., Hanchar, J.M., Horstwood, M.S.A., Morris, G.A., Nasdala, L., Norberg, N., Schaltegger, U., Schoene, B., Tubrett, M.N. and Whitehouse, M.J., 2008. Plešovice zircon - a new natural reference material for U-Pb and Hf isotopic microanalysis. Chemical Geology, 249, 1-35.

Stacey, J.S. and Kramers, J.D., 1975. Approximation of terrestrial lead isotope evolution by a two-stage model. Earth and Planetary Science Letters, 26, 207-221.

Ziegler, P., 1990. Geological Atlas of Western and Central Europe. Shell Internationale Petroleum Maatschappij BV, London.

Table 1. Composition of heavy mineral separates in the 63-125 μm fraction of ditch cuttings samples from A05-1 and A15-1, expressed as frequency % on a count of 200 grains.

Well	Depth (ft)	Depth (m)	HM	OP	CB	BY	FL	AH	SF	MC
A05-1	10250	3124		6.0	3.0	86.0	0.5			4.5
	10270	3130	0.5	8.5	2.5	84.5	1.0			3.0
	10280	3133	0.5	13.0	1.0	84.0	1.0			0.5
	10290	3136		10.0	4.5	84.0	1.5			
	10310	3143	0.5	12.0	2.0	84.5	0.5			0.5
	10320	3146		5.0	2.0	91.5	1.0			0.5
	10340	3152		3.5	1.5	94.0	0.5			0.5
	10350	3155		5.5	0.5	93.5	0.5			
	10360	3158		6.5	2.5	90.0	1.0			
	10370	3161		4.0	3.0	91.5	0.5			1.0
	10390	3167	0.5	7.0	5.0	86.0	1.0		0.5	
	10420	3176	0.5	11.5	2.5	83.0	1.5			1.0
	10440	3182	0.5	7.0	3.0	88.5				1.0
A15-1	9650	2941		2.5	91.0	5.0		1.0		0.5
	9660	2944		4.0	89.5	4.0		1.0		1.5
	9680	2950		2.0	93.5	3.5		1.0		
	9690	2954		3.5	84.0	8.5		1.5		2.5
	9710	2960	1.5	6.0	83.0	7.0		1.5		1.0
	9730	2966	0.5	6.5	77.0	11.5		2.0		2.5
	9740	2969	1.0	6.5	77.0	7.5	0.5	6.5		1.0
	9770	2978	0.5	9.0	79.5	9.5		1.0		0.5
	9780	2981	0.5	5.0	77.0	14.5	0.5	2.0		0.5
	9790	2984	1.0	12.5	72.5	13.0	0.5	0.5		
	9800	2987	1.0	12.5	74.0	11.5	0.5	0.5		
	9820	2993	2.0	15.0	66.0	16.5		0.5		
	9830	2996	1.5	6.5	80.0	10.5		1.5		

HM – non-opaque detrital heavy minerals, OP – opaques and semi-opaques, CB – carbonate, BY – barite, AH – anhydrite, SF – sphalerite, MC – mica and chlorite

Table 2. Relative abundance of detrital non-opaque heavy minerals in the 63-125 μm fraction of samples from A05-1 and A15-1, expressed as frequency %. Data in parentheses refer to raw grain counts for samples with poor recovery.

Well	Depth (ft)	Depth (m)	At	Ap	Ca	Cp	Ep	Gt	Op	Ru	Sp	St	To	Zr	total
A05-1	10250	3124	0.5	36.0	1.5	1.0	1.0	4.0	1.0	7.0			23.0	25.0	200
	10270	3130		40.7	5.9	5.9	2.0	7.9		3.0		1.0	26.7	6.9	101
	10280	3133	2.5	18.5	0.5	1.0	1.0	19.5	0.5	5.5			8.5	42.5	200
	10290	3136	3.6	25.0	10.7	7.1				3.6			17.9	32.1	28
	10310	3143	0.9	46.7	0.9	1.9	0.9	2.8	1.9	5.6			22.4	16.0	107
	10320	3146	1.6	37.7	1.6	1.6		8.2		3.3			16.4	29.6	61
	10340	3152	1.0	43.3	3.1			8.2		6.2			12.4	25.8	97
	10350	3155		45.5	1.8		3.5	5.3	3.5	5.3			10.5	24.6	57
	10360	3158		38.5	3.1	4.6	3.1	9.2		4.6			12.3	24.6	65
	10370	3161	2.6	30.8	3.8			2.6		3.8			24.4	32.0	78
	10390	3167	1.3	45.5	5.1	1.3		3.8		2.5			17.7	22.8	79
	10420	3176	2.2	35.9	1.1	1.7	0.6	5.5		4.4	0.6		9.4	38.6	181
	10440	3182		53.8	1.7	1.2		2.9		4.0			7.5	28.9	173
A15-1	9650	2941		62.9				5.7		5.7			5.7	20.0	35
	9660	2944	3.7	55.6	3.7			7.4		3.7			25.9		27
	9680	2950		(6)									(2)		8
	9690	2954		70.0	5.0			5.0					10.0	10.0	20
	9710	2960	1.5	55.2				6.0					6.0	31.3	67
	9730	2966	2.0	50.0	1.0			7.0		1.0			15.0	24.0	100
	9740	2969		66.7									8.8	24.5	57
	9770	2978		29.5				4.5					18.2	47.8	88
	9780	2981	2.2	41.6	1.1			3.4		2.2			12.4	37.1	89
	9790	2984	2.8	41.0				6.9		2.8			14.6	31.9	144
	9800	2987	2.9	36.3				1.0		2.0			13.7	44.1	102
	9820	2993	1.0	42.0			0.5	4.0		2.0		0.5	12.0	38.0	200
	9830	2996	1.4	28.4				2.8		0.7			17.0	49.7	141

At - anatase, Ap – apatite, Ca – calcic amphibole, Cp - clinopyroxene, Ep – epidote, Gt – garnet, Op – orthopyroxene, Ru – rutile, Sp – titanite, St – staurolite, To – tourmaline, Zr – zircon

Table 3. Provenance-sensitive indices from A05-1 and A15-1. Data in parentheses refer to raw grain counts for samples with poor recovery.

Well	Depth (ft)	Depth (m)	ATi	total	GZi	total	RuZi	total	MZi	total	CZi	total	ZAi	total	ARi	total
A05-1	10250	3124	59.7	129	13.1	61	22.1	68	0.0	53	0.0	53	40.8	130	24.7	77
	10270	3130	60.3	68	(8/15)		(3/10)		(0/7)		(0/7)		14.6	48	29.3	41
	10280	3133	71.4	70	29.1	141	9.9	111	0.0	100	0.0	100	66.0	147	32.0	50
	10290	3136	(7/12)		(0/9)		(1/10)		(0/9)		(0/9)		(9/16)		(3/7)	
	10310	3143	67.6	74	15.0	20	26.1	23	(0/17)		(0/17)		25.4	67	30.0	50
	10320	3146	69.7	33	21.7	23	10.0	20	(0/18)		(0/18)		43.9	41	47.8	23
	10340	3152	77.8	54	24.2	33	19.4	31	0.0	25	0.0	25	37.3	67	52.4	42
	10350	3155	70.0	20	(3/17)		(3/17)		(0/14)		(0/14)		35.0	40	33.3	27
	10360	3158	75.8	33	27.3	22	(3/19)		(0/16)		(0/16)		39.0	41	32.0	25
	10370	3161	55.8	43	10.7	28	10.7	28	0.0	25	0.0	25	51.0	49	41.7	24
	10390	3167	72.0	50	14.3	21	10.0	20	(0/18)		(0/18)		33.3	54	55.6	36
	10420	3176	79.3	82	12.5	80	10.3	78	0.0	70	0.0	70	51.9	135	50.8	65
	10440	3182	87.7	106	9.1	55	12.3	57	0.0	50	0.0	50	35.0	143	61.3	93
A15-1	9650	2941	91.7	24	(2/9)		(2/9)		(0/7)		(0/7)		24.1	29	54.5	22
	9660	2944	68.2	22	(2/2)		(1/1)						(0/15)		(9/15)	
	9680	2950	(6/8)												(3/6)	
	9690	2954	(14/16)		(1/3)		(0/2)		(0/2)		(0/2)		(2/16)		(9/14)	
	9710	2960	90.2	41	0.0	21	0.0	21	0.0	21	0.0	21	36.2	58	59.5	37
	9730	2966	76.9	65	22.6	31	4.0	25	0.0	24	0.0	24	32.4	74	64.0	50
	9740	2969	88.4	43	(0/14)		(0/14)		(0/14)		(0/14)		26.9	52	60.5	38
	9770	2978	61.9	42	8.7	46	0.0	42	0.0	42	0.0	42	61.8	68	53.8	26
	9780	2981	77.1	48	8.3	36	5.7	35	0.0	33	0.0	33	47.1	70	51.4	37
	9790	2984	73.8	80	17.9	56	8.0	50	0.0	46	0.0	46	44.7	103	45.8	59
	9800	2987	72.5	51	2.2	46	4.3	47	0.0	45	0.0	45	54.9	82	51.4	37
	9820	2993	78.7	127	10.3	97	4.4	91	0.0	87	0.0	87	47.5	160	52.0	100
	9830	2996	62.5	64	5.4	74	1.4	71	0.0	70	0.0	70	63.6	110	57.5	40

ATi – apatite:tourmaline index (% apatite in total apatite plus tourmaline)
GZi – garnet:zircon index (% garnet in total garnet plus zircon)
RuZi – rutile:zircon index (% rutile in total rutile plus zircon)
MZi – monazite:zircon index (% monazite in total monazite plus zircon)
CZi – chrome spinel:zircon index (% chrome spinel in total chrome spinel plus zircon)
ARi – apatite roundness index ((% rounded apatite in total apatite population)

Table 4. LA-SF-ICP-MS U-Th-Pb zircon dating methodology at CAF, Stellenbosch University

Laboratory & Sample Preparation	
Laboratory name	Central Analytical Facility, Stellenbosch University
Sample type / mineral	Detrital and magmatic zircons
Sample preparation	Conventional mineral separation, 1 inch resin mount, 1 µm polish to finish
Imaging	CL, LEO 1430 VP, 10 nA, 15 mm working distance
Laser ablation system	
Make, Model & type	ESI/New Wave Research, UP213, Nd:YAG
Ablation cell & volume	Custom build low volume cell, volume ca.3 cm^3
Laser wavelength	213 nm
Pulse width	3 ns
Fluence	2.5 J/cm^{-2}
Repetition rate	10 Hz
Spot size	30 µm
Sampling mode / pattern	30 µm single spot analyses
Carrier gas	100% He, Ar make-up gas combined using a T-connector close to sample cell
Pre-ablation laser warm-up (background collection)	40 seconds
Ablation duration	20 seconds
Wash-out delay	30 seconds
Cell carrier gas flow	0.3 l/min He
ICP-MS Instrument	
Make, Model & type	Thermo Finnigan Element2 single collector HR-SF-ICP-MS
Sample introduction	Via conventional tubing
RF power	1100 W
Make-up gas flow	1.0 l/min Ar
Detection system	Single collector secondary electron multiplier
Masses measured	202, 204, 206, 207, 208, 232, 233, 235, 238
Integration time per peak	4 ms
Total integration time per reading	Approx. 1 sec
Sensitivity	20000 cps/ppm Pb
Dead time	16 ns
Data Processing	
Gas blank	40 second on-peak
Calibration strategy	GJ-1 used as primary reference material, Plešovice and M127 used as secondary reference material (Quality Control)
Reference Material info	M127 (Nasdala et al., 2008; Mattinson, 2010); Plešovice (Slama et al., 2008); GJ-1 (Jackson et al., 2004)
Data processing package used / Correction for LIEF	In-house spreadsheet data processing using intercept method for laser induced elemental fractionation (LIEF) correction
Mass discrimination	Standard-sample bracketing with $^{207}Pb/^{206}Pb$ and $^{206}Pb/^{238}U$ normalised to reference material GJ-1
Common-Pb correction, composition and uncertainty	204-method, Stacey and Kramers (1975) composition at the projected age of the mineral, 5% uncertainty assigned
Uncertainty level & propagation	Ages are quoted at 2 sigma absolute, propagation is by quadratic addition. Reproducibility and age uncertainty of reference material and common-Pb composition uncertainty are propagated.
Quality control / Validation	Plešovice: Wtd ave $^{206}Pb/^{238}U$ age = 337 ± 4 (2SD, MSWD = 0.2) M127: Wtd ave $^{206}Pb/^{238}U$ age = 520 ± 5 (2SD, MSWD = 0.8)
Other information	Detailed method description reported by Frei and Gerdes (2009)

Table 5. U-Pb isotopic compositions and ages of zircons from A15-1, 9770-9820 ft.

					RATIOS							AGES						CONC
Analysis	U [ppm][a]	Pb [ppm][a]	$^{206}Pb/^{204}Pb$	Th/U[a]	$^{207}Pb/^{235}U$[b]	2 σ[d]	$^{206}Pb/^{238}U$[b]	2 σ[d]	rho[c]	$^{207}Pb/^{206}Pb$[e]	2 σ[d]	$^{207}Pb/^{235}U$	2 σ	$^{206}Pb/^{238}U$	2 σ	$^{207}Pb/^{206}Pb$	2 σ	%
A_276	33	4	1786	1.72	1.330	0.072	0.1170	0.0039	0.62	0.0824	0.0035	859	47	713	24	1256	84	57
A_277	18	1	77	1.28	0.330	0.078	0.0461	0.0018	0.17	0.0519	0.0120	290	68	291	12	283	530	103
A_278	179	34	5538	0.37	2.096	0.086	0.1923	0.0061	0.77	0.0791	0.0021	1148	47	1134	36	1174	52	97
A_279	165	33	2897	0.19	2.172	0.087	0.1993	0.0063	0.79	0.0791	0.0019	1172	47	1171	37	1174	48	100
A_280	156	9	1071	0.02	0.402	0.026	0.0546	0.0019	0.52	0.0535	0.0030	343	23	342	12	349	127	98
A_281	114	36	139270	0.43	4.638	0.182	0.3140	0.0099	0.81	0.1071	0.0025	1756	69	1760	56	1751	42	101
A_282	274	57	10351	0.35	2.328	0.091	0.2065	0.0065	0.81	0.0818	0.0019	1221	48	1210	38	1240	45	98
A_283	631	135	2626	0.56	3.232	0.123	0.2132	0.0067	0.83	0.1099	0.0023	1465	56	1246	39	1798	38	69
A_284	449	117	6363	0.84	3.410	0.132	0.2607	0.0082	0.82	0.0949	0.0021	1507	58	1493	47	1526	42	98
A_285	139	42	164494	0.42	4.364	0.170	0.3043	0.0096	0.81	0.1040	0.0024	1706	66	1712	54	1697	42	101
A_286	546	95	32047	0.20	1.734	0.067	0.1731	0.0055	0.82	0.0727	0.0016	1021	39	1029	32	1005	45	102
A_287	238	53	13009	0.32	2.591	0.101	0.2218	0.0070	0.81	0.0847	0.0019	1298	51	1291	41	1309	44	99
A_288	231	58	11337	0.42	3.178	0.124	0.2523	0.0080	0.81	0.0914	0.0021	1452	57	1450	46	1454	44	100
A_289	119	30	118220	0.53	3.242	0.129	0.2544	0.0081	0.80	0.0924	0.0022	1467	58	1461	46	1476	46	99
A_290	91	23	4852	0.46	3.194	0.136	0.2533	0.0081	0.75	0.0915	0.0026	1456	62	1456	47	1456	53	100
A_293	180	19	75187	0.75	0.914	0.039	0.1071	0.0034	0.75	0.0619	0.0017	659	28	656	21	671	59	98
A_294	315	22	4133	0.52	0.539	0.023	0.0700	0.0022	0.75	0.0558	0.0015	438	18	436	14	446	61	98
A_295	465	33	2583	0.35	0.537	0.022	0.0700	0.0022	0.78	0.0556	0.0014	436	18	436	14	437	57	100
A_296	191	39	151446	0.69	2.266	0.089	0.2034	0.0064	0.80	0.0808	0.0019	1202	47	1194	38	1216	46	98
A_297	656	102	2155	0.59	2.114	0.081	0.1557	0.0049	0.83	0.0985	0.0021	1153	44	933	29	1595	40	58
A_298	318	60	174539	0.34	1.988	0.077	0.1887	0.0060	0.81	0.0764	0.0017	1112	43	1115	35	1106	46	101
A_299	305	78	26722	0.22	3.462	0.133	0.2567	0.0081	0.82	0.0978	0.0021	1519	58	1473	46	1583	41	93
A_300	114	5	377	0.45	0.331	0.018	0.0462	0.0015	0.59	0.0520	0.0023	290	16	291	10	285	102	102
A_301	713	39	11863	0.12	0.398	0.016	0.0541	0.0017	0.78	0.0533	0.0014	340	14	340	11	340	59	100
A_302	291	85	5215	0.24	4.114	0.158	0.2936	0.0093	0.83	0.1016	0.0022	1657	63	1659	52	1654	40	100
A_303	253	65	2483	0.47	3.587	0.138	0.2579	0.0082	0.82	0.1009	0.0022	1547	60	1479	47	1641	41	90
A_304	34	2	6558	1.01	0.377	0.049	0.0492	0.0021	0.34	0.0556	0.0068	325	42	309	13	437	271	71
A_305	66	14	52993	0.61	2.308	0.103	0.2072	0.0067	0.73	0.0808	0.0025	1215	54	1214	39	1216	60	100
A_306	417	86	5196	0.65	2.839	0.109	0.2066	0.0065	0.82	0.0997	0.0022	1366	52	1211	38	1618	40	75
A_307	624	121	32475	0.40	2.376	0.091	0.1945	0.0061	0.83	0.0886	0.0019	1235	47	1145	36	1396	41	82
A_310	65	11	41877	0.63	1.674	0.077	0.1665	0.0054	0.71	0.0729	0.0024	999	46	993	32	1011	66	98
A_311	591	49	1454	0.70	0.676	0.041	0.0831	0.0028	0.56	0.0590	0.0030	524	32	514	17	568	109	91
A_312	62	32	79153	1.27	12.950	0.516	0.5162	0.0165	0.80	0.1820	0.0043	2676	107	2683	86	2671	39	100
A_313	65	12	2308	0.52	1.982	0.093	0.1887	0.0061	0.69	0.0762	0.0026	1110	52	1114	36	1100	68	101
A_314	198	103	400671	0.19	14.098	0.574	0.5216	0.0168	0.79	0.1960	0.0049	2756	112	2706	87	2793	41	97
A_316	139	37	143709	0.41	3.504	0.138	0.2667	0.0085	0.80	0.0953	0.0022	1528	60	1524	48	1534	44	99
A_317	111	22	2551	0.29	2.230	0.093	0.2027	0.0065	0.77	0.0798	0.0021	1191	50	1190	38	1192	53	100
A_318	61	19	1623	0.56	4.807	0.196	0.3196	0.0102	0.78	0.1091	0.0028	1786	73	1788	57	1784	46	100
A_319	138	25	8951	0.63	1.919	0.078	0.1827	0.0058	0.78	0.0762	0.0019	1088	44	1082	34	1100	51	98
A_320	207	49	3754	0.38	2.874	0.114	0.2353	0.0075	0.80	0.0886	0.0021	1375	55	1362	43	1395	45	98
A_321	180	53	7871	0.66	4.153	0.162	0.2942	0.0093	0.81	0.1024	0.0023	1665	65	1662	53	1668	42	100
A_322	261	18	2318	0.14	0.513	0.030	0.0672	0.0022	0.58	0.0553	0.0026	420	24	419	14	426	106	98
A_323	163	52	11486	0.27	5.081	0.197	0.3222	0.0102	0.82	0.1144	0.0026	1833	71	1800	57	1870	40	96
A_324	186	13	2150	0.72	0.548	0.025	0.0717	0.0023	0.71	0.0555	0.0018	444	20	446	14	432	71	103
A_327	70	12	47793	0.39	1.791	0.079	0.1755	0.0057	0.73	0.0740	0.0022	1042	46	1043	34	1041	61	100
A_328	170	43	5194	0.25	3.192	0.126	0.2523	0.0080	0.81	0.0918	0.0021	1455	57	1450	46	1463	44	99
A_329	81	26	20520	0.47	4.803	0.199	0.3200	0.0103	0.77	0.1089	0.0029	1785	74	1790	57	1780	48	101
A_330	350	74	287891	0.40	2.408	0.094	0.2121	0.0067	0.81	0.0823	0.0019	1245	49	1240	39	1253	45	99

Table 5 (continued).

					RATIOS							AGES						CONC
Analysis	U [ppm][a]	Pb [ppm][a]	$^{206}Pb/^{204}Pb$	Th/U[a]	$^{207}Pb/^{235}U$[b]	2 σ[d]	$^{206}Pb/^{238}U$[b]	2 σ[d]	rho[c]	$^{207}Pb/^{206}Pb$[e]	2 σ[d]	$^{207}Pb/^{235}U$	2 σ	$^{206}Pb/^{238}U$	2 σ	$^{207}Pb/^{206}Pb$	2 σ	%
A_331	203	33	128694	0.35	1.609	0.065	0.1631	0.0052	0.79	0.0715	0.0018	974	39	974	31	973	51	100
A_332	690	168	68474	0.31	3.039	0.116	0.2430	0.0077	0.83	0.0907	0.0020	1417	54	1402	44	1440	41	97
A_333	168	39	9732	0.39	2.731	0.111	0.2305	0.0074	0.78	0.0860	0.0022	1337	55	1337	43	1337	49	100
A_334	58	11	41982	0.29	1.951	0.087	0.1860	0.0060	0.72	0.0761	0.0024	1099	49	1100	36	1097	62	100
A_335	177	32	8343	0.42	1.870	0.075	0.1805	0.0057	0.79	0.0752	0.0019	1071	43	1070	34	1073	50	100
A_336	86	26	8957	0.47	4.474	0.197	0.3053	0.0099	0.74	0.1063	0.0032	1726	76	1718	56	1737	55	99
A_337	138	45	173721	0.46	4.975	0.195	0.3246	0.0103	0.81	0.1112	0.0026	1815	71	1812	58	1818	42	100
A_338	157	26	3918	0.44	1.657	0.072	0.1667	0.0054	0.74	0.0721	0.0021	992	43	994	32	988	60	101
A_339	102	17	7020	0.31	1.716	0.073	0.1711	0.0055	0.76	0.0727	0.0020	1014	43	1018	33	1006	56	101
A_340	85	22	2735	0.62	3.426	0.146	0.2633	0.0085	0.75	0.0944	0.0026	1510	64	1507	49	1515	53	99
A_341	346	76	7198	0.55	2.500	0.097	0.2185	0.0069	0.82	0.0830	0.0019	1272	49	1274	40	1268	44	100
A_349	57	15	2571	0.23	3.349	0.142	0.2586	0.0083	0.76	0.0939	0.0026	1493	63	1482	48	1507	52	98
A_350	97	17	66443	0.59	1.859	0.079	0.1766	0.0057	0.76	0.0764	0.0021	1067	45	1048	34	1104	56	95
A_351	324	93	9434	0.55	3.961	0.153	0.2875	0.0091	0.82	0.0999	0.0022	1626	63	1629	52	1623	41	100
A_352	185	40	5059	0.12	2.483	0.103	0.2159	0.0069	0.77	0.0834	0.0022	1267	52	1260	40	1279	51	99
A_353	47	8	907	0.73	1.847	0.087	0.1776	0.0058	0.69	0.0754	0.0026	1063	50	1054	34	1080	69	98
A_354	143	38	147506	0.37	3.470	0.138	0.2661	0.0085	0.80	0.0946	0.0022	1520	60	1521	48	1520	45	100
A_355	159	30	3101	0.27	2.027	0.083	0.1916	0.0061	0.78	0.0767	0.0020	1124	46	1130	36	1113	52	102
A_356	174	33	128546	0.47	2.054	0.083	0.1904	0.0061	0.79	0.0782	0.0019	1134	46	1124	36	1153	49	97
A_357	165	34	2392	0.33	2.257	0.092	0.2043	0.0065	0.78	0.0801	0.0020	1199	49	1199	38	1199	50	100
A_358	67	17	14193	0.45	3.135	0.132	0.2496	0.0080	0.76	0.0911	0.0025	1441	61	1436	46	1449	52	99
A_361	192	43	166179	0.42	2.631	0.116	0.2229	0.0072	0.74	0.0856	0.0025	1309	58	1297	42	1329	57	98
A_362	459	72	5868	0.32	1.539	0.061	0.1565	0.0050	0.80	0.0714	0.0017	946	37	937	30	968	48	97
A_363	1708	94	13712	0.07	0.407	0.016	0.0549	0.0017	0.80	0.0538	0.0013	347	14	344	11	363	53	95
A_364	47	7	576	0.71	1.569	0.111	0.1587	0.0057	0.51	0.0717	0.0044	958	68	949	34	978	124	97
A_365	117	22	86110	0.21	2.047	0.085	0.1907	0.0061	0.77	0.0778	0.0021	1131	47	1125	36	1143	53	98
A_366	375	89	346002	0.30	2.926	0.114	0.2380	0.0076	0.82	0.0892	0.0020	1389	54	1376	44	1408	43	98
A_367	122	40	154130	0.35	4.928	0.195	0.3252	0.0104	0.81	0.1099	0.0026	1807	72	1815	58	1798	43	101
A_368	26	4	16344	0.65	1.626	0.111	0.1618	0.0058	0.52	0.0729	0.0043	980	67	967	34	1011	118	96
A_369	154	31	120207	0.46	2.352	0.098	0.2021	0.0065	0.77	0.0844	0.0022	1228	51	1186	38	1303	52	91
A_370	199	37	3701	0.32	1.973	0.079	0.1851	0.0059	0.79	0.0773	0.0019	1106	45	1095	35	1129	49	97
A_371	342	68	10546	0.36	2.206	0.087	0.2001	0.0064	0.80	0.0800	0.0019	1183	47	1176	37	1196	46	98
A_372	211	9	36551	0.76	0.329	0.022	0.0448	0.0015	0.51	0.0533	0.0031	289	19	283	10	340	130	83
A_373	36	3	11792	0.70	0.666	0.062	0.0835	0.0032	0.41	0.0579	0.0049	518	49	517	20	525	187	98
A_374	314	81	71056	0.48	3.300	0.129	0.2584	0.0082	0.81	0.0926	0.0021	1481	58	1482	47	1480	43	100
A_375	82	22	4791	1.01	3.621	0.156	0.2711	0.0088	0.75	0.0969	0.0027	1554	67	1546	50	1565	53	99
A_378	189	29	9967	0.30	1.452	0.060	0.1512	0.0048	0.77	0.0696	0.0018	911	38	908	29	917	54	99
A_379	202	52	22832	0.57	3.300	0.133	0.2578	0.0082	0.79	0.0929	0.0023	1481	60	1478	47	1485	47	100
A_380	157	48	29117	0.43	4.404	0.174	0.3050	0.0097	0.80	0.1047	0.0025	1713	68	1716	55	1709	43	100
A_381	102	29	15026	0.27	4.054	0.165	0.2898	0.0093	0.79	0.1015	0.0025	1645	67	1641	53	1651	46	99
A_382	377	28	13826	0.37	0.591	0.025	0.0755	0.0024	0.76	0.0568	0.0015	471	20	469	15	483	60	97
A_383	132	29	2835	0.51	2.493	0.103	0.2176	0.0070	0.78	0.0831	0.0022	1270	52	1269	41	1272	51	100
A_384	557	117	11618	0.34	2.363	0.092	0.2103	0.0067	0.82	0.0815	0.0018	1231	48	1230	39	1233	44	100
A_385	1159	204	5138	0.71	2.286	0.089	0.1762	0.0056	0.82	0.0941	0.0021	1208	47	1046	33	1510	42	69
A_386	82	21	3289	0.54	3.238	0.135	0.2545	0.0082	0.77	0.0923	0.0024	1466	61	1462	47	1473	50	99
A_387	144	27	9245	0.35	2.011	0.083	0.1913	0.0061	0.78	0.0763	0.0020	1119	46	1128	36	1102	52	102
A_388	2099	220	1050	1.23	1.536	0.059	0.1050	0.0033	0.82	0.1061	0.0023	945	37	644	20	1734	40	37
A_389	455	143	553003	0.64	4.708	0.183	0.3143	0.0100	0.82	0.1086	0.0024	1769	69	1762	56	1776	41	99

Table 5 (continued).

					RATIOS							AGES						CONC
Analysis	U [ppm][a]	Pb [ppm][a]	$^{206}Pb/^{204}Pb$	Th/U[a]	$^{207}Pb/^{235}U$[b]	2 σ[d]	$^{206}Pb/^{238}U$[b]	2 σ[d]	rho[c]	$^{207}Pb/^{206}Pb$[e]	2 σ[d]	$^{207}Pb/^{235}U$	2 σ	$^{206}Pb/^{238}U$	2 σ	$^{207}Pb/^{206}Pb$	2 σ	%
A_390	93	17	63900	0.30	1.831	0.082	0.1785	0.0058	0.72	0.0744	0.0023	1057	48	1059	34	1052	63	101
A_391	106	33	126612	0.58	4.588	0.185	0.3104	0.0099	0.79	0.1072	0.0026	1747	70	1743	56	1752	45	99
A_392	74	11	1342	0.42	1.489	0.068	0.1547	0.0050	0.71	0.0698	0.0022	926	42	927	30	923	65	100
A_395	70	12	47057	0.24	1.772	0.080	0.1738	0.0056	0.72	0.0740	0.0023	1035	47	1033	34	1040	63	99
A_396	41	8	30678	0.46	2.034	0.122	0.1914	0.0066	0.58	0.0771	0.0038	1127	67	1129	39	1123	97	101
A_397	61	21	80761	0.78	5.416	0.225	0.3399	0.0110	0.77	0.1156	0.0030	1887	79	1886	61	1889	47	100
A_398	111	32	123971	0.76	3.978	0.161	0.2889	0.0092	0.79	0.0999	0.0025	1630	66	1636	52	1621	46	101
A_399	44	10	6272	0.56	2.600	0.119	0.2219	0.0072	0.71	0.0850	0.0027	1301	59	1292	42	1315	62	98
A_400	82	18	2650	0.66	2.572	0.129	0.2214	0.0074	0.66	0.0843	0.0032	1293	65	1289	43	1298	73	99
A_401	66	12	47428	0.26	1.977	0.090	0.1863	0.0061	0.72	0.0770	0.0024	1108	50	1101	36	1120	63	98
A_402	128	34	22847	0.32	3.481	0.143	0.2662	0.0085	0.78	0.0948	0.0024	1523	63	1521	49	1525	48	100
A_403	109	32	928	0.12	4.483	0.201	0.2920	0.0096	0.73	0.1114	0.0034	1728	78	1651	54	1822	56	91
A_404	123	65	250616	0.79	13.582	0.539	0.5274	0.0169	0.81	0.1868	0.0044	2721	108	2731	87	2714	39	101
A_405	131	23	1167	0.50	1.830	0.077	0.1773	0.0057	0.76	0.0749	0.0020	1056	45	1052	34	1065	55	99
A_406	137	21	2150	0.38	1.472	0.065	0.1541	0.0050	0.74	0.0693	0.0021	919	40	924	30	907	61	102
A_407	59	9	5325	0.67	1.603	0.079	0.1591	0.0052	0.67	0.0731	0.0027	971	48	952	31	1016	75	94
A_408	43	13	1536	0.58	4.425	0.207	0.3029	0.0100	0.71	0.1060	0.0035	1717	80	1705	56	1731	61	99
A_409	43	13	51969	0.68	4.570	0.234	0.3099	0.0105	0.66	0.1070	0.0041	1744	89	1740	59	1748	71	100

[a]U and Pb concentrations and Th/U ratios are calculated relative to GJ-1 reference zircon

[b]Corrected for background and within-run Pb/U fractionation and normalised to reference zircon GJ-1 (ID-TIMS values/measured value); 207Pb/235U calculated using ($^{207}Pb/^{206}Pb$)/($^{238}U/^{206}Pb$ * 1/137.88)

[c]Rho is the error correlation defined as the quotient of the propagated errors of the $^{206}Pb/^{238}U$ and the $^{207}Pb/^{235}U$ ratio

[d]Quadratic addition of within-run errors (2 SD) and daily reproducibility of GJ-1 (2 SD)

[e]Corrected for mass-bias by normalising to GJ-1 reference zircon (~0.6 per atomic mass unit) and common Pb using the model Pb composition of Stacey and Kramers (1975)

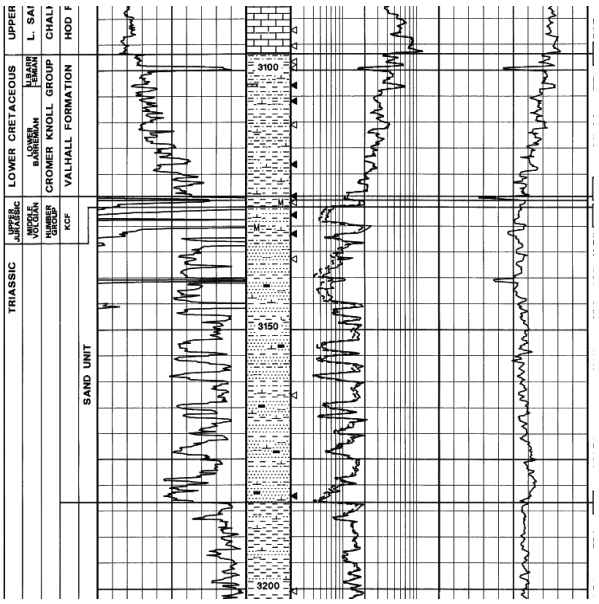

A05-01

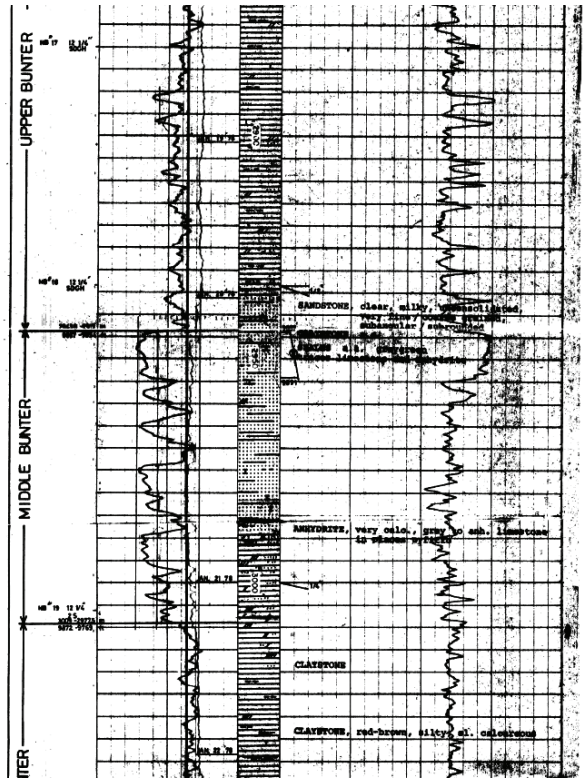

A15-01

Fig. 1. Composite logs over the intervals analysed from the two wells used in this study

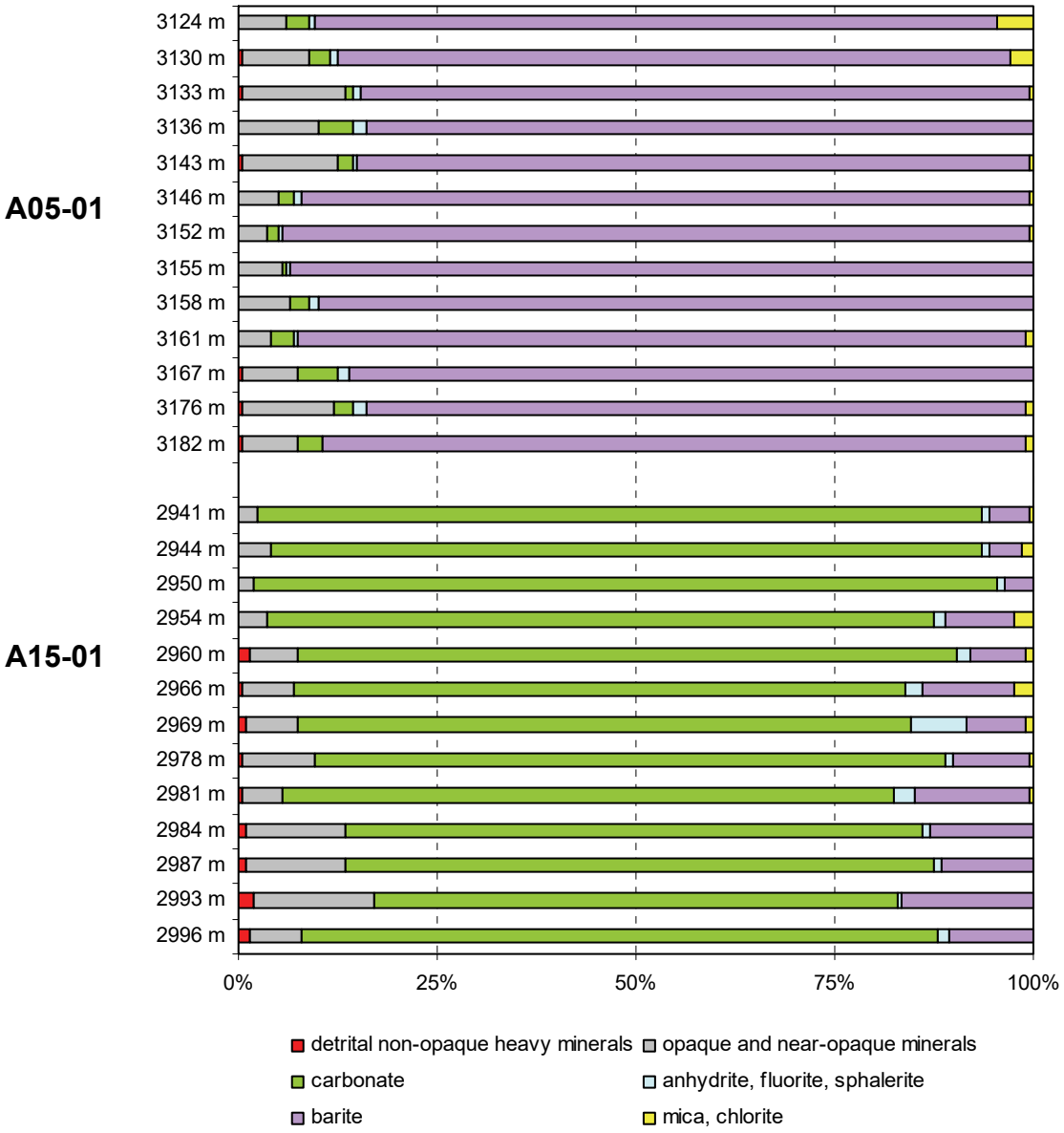

Fig. 2. Composition of heavy mineral separates from A05-01 and A15-01

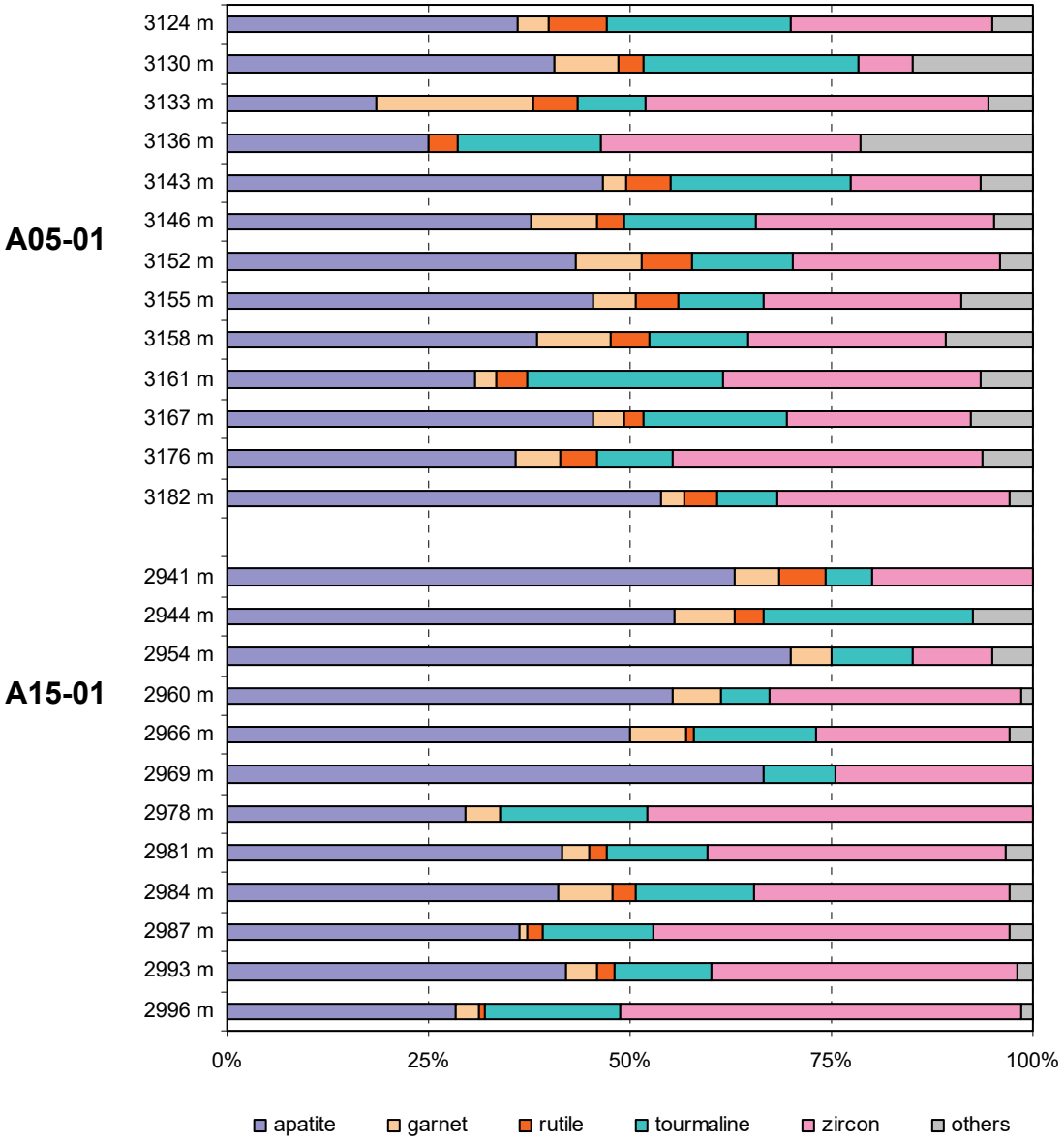

Fig. 3. Detrital non-opaque heavy mineral assemblage compositions in A05-01 and A15-01

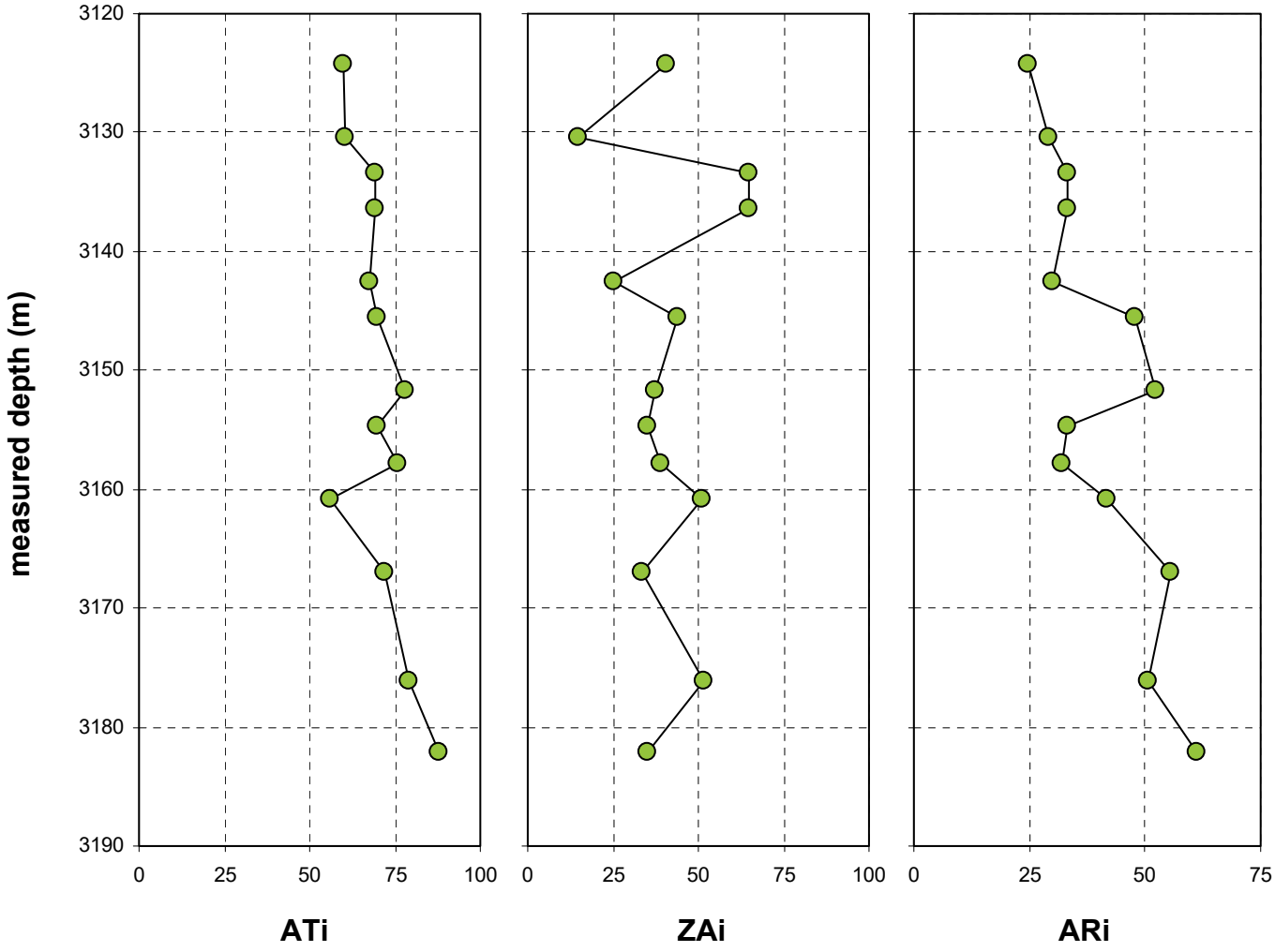

Fig. 4. Stratigraphic variations in heavy mineral index parameters in A05-01.

Note that data are pooled at 3133-3136 m owing to low grain counts in individual samples.

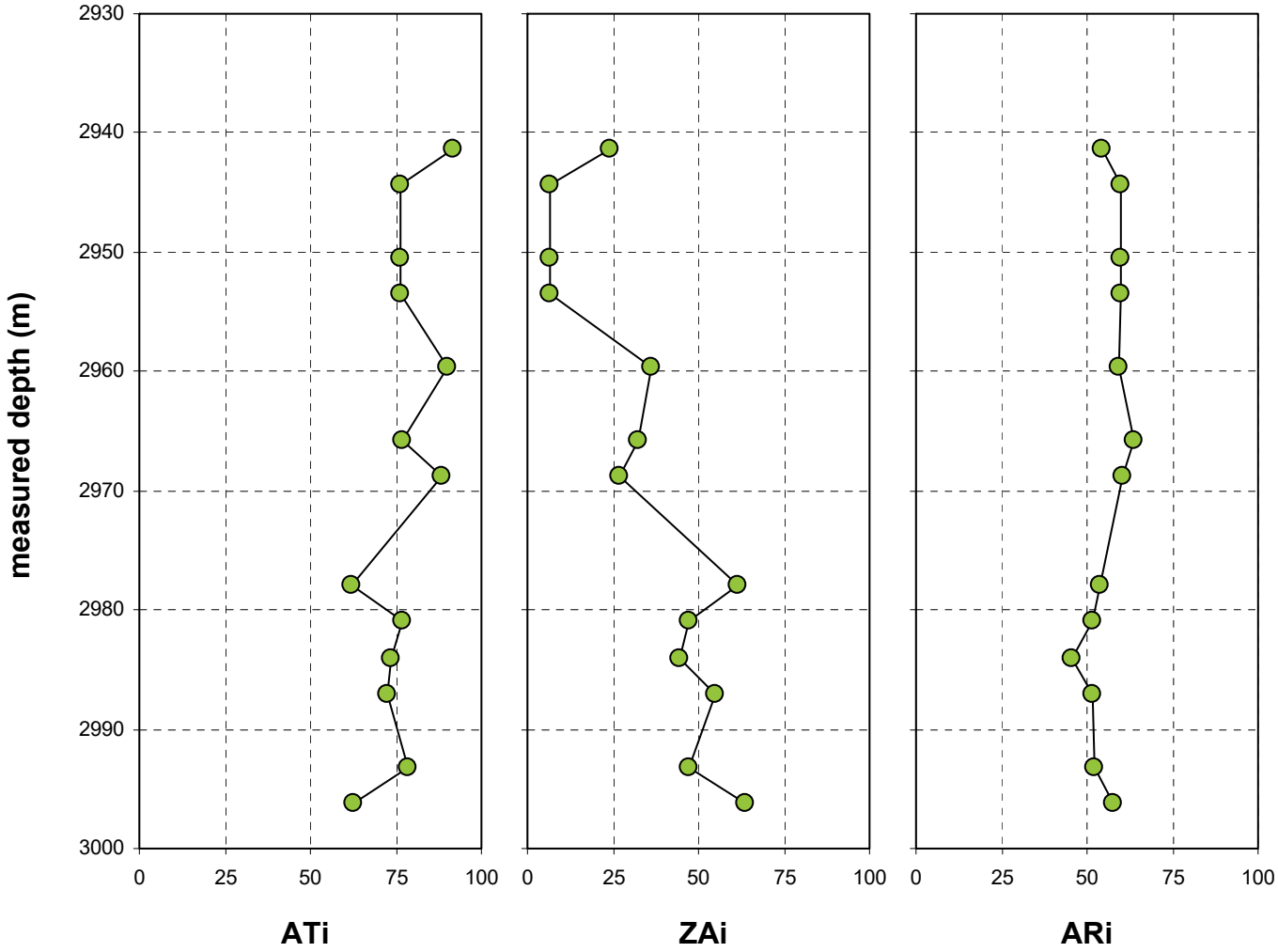

Fig. 5. Stratigraphic variations in heavy mineral index parameters in A15-01.

Note that data are pooled at 2944-2954 m owing to low grain counts in individual samples.

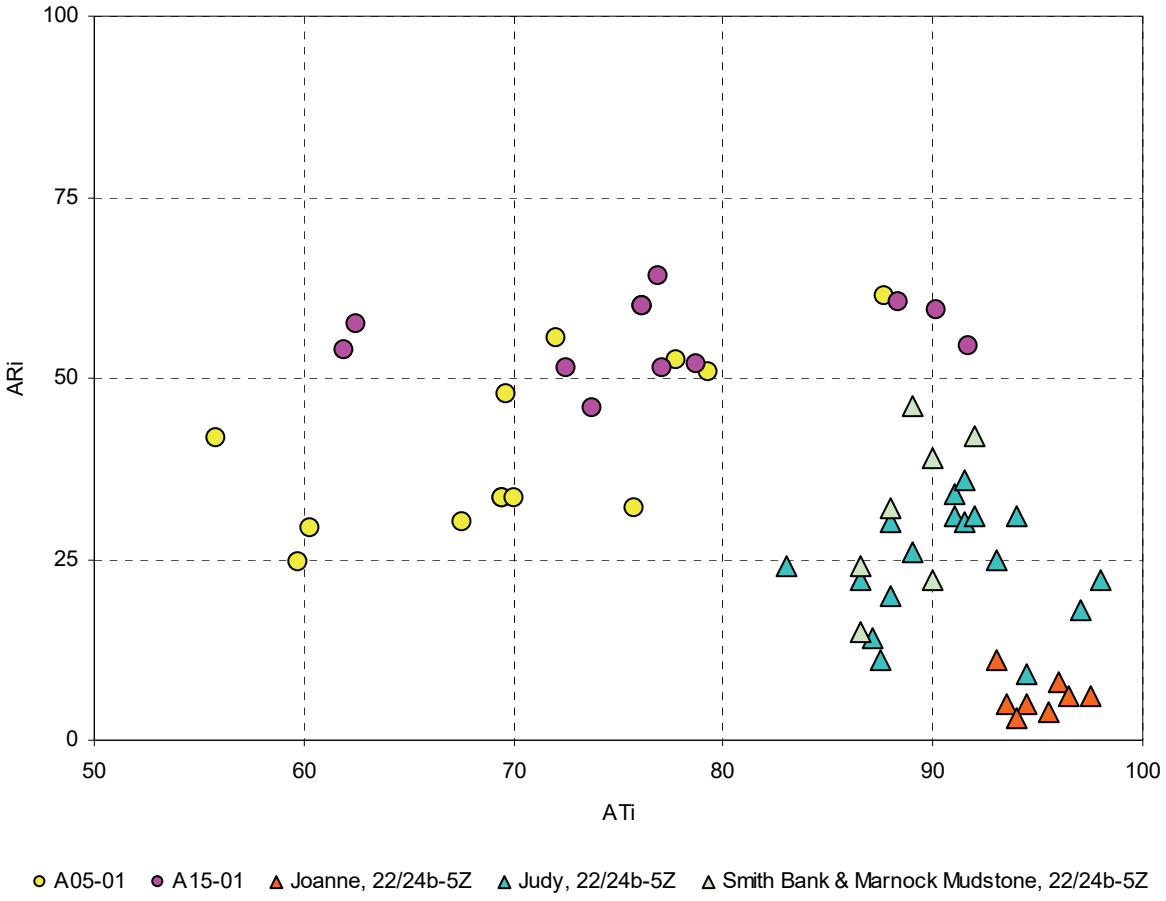

Fig. 6. Crossplot of apatite:tourmaline index (ATi) and apatite roundness index (ARi) in A05-01 and A15-01, showing overlap between the two wells that suggests a common provenance.

The Dutch sector data are compared with the Triassic in UK Quadrant 22, central North Sea, using Marnock Field well 22/24b-5Z (Mouritzen et al., 2017). There is no overlap between the two areas, especially at the younger Joanne sandstone level.

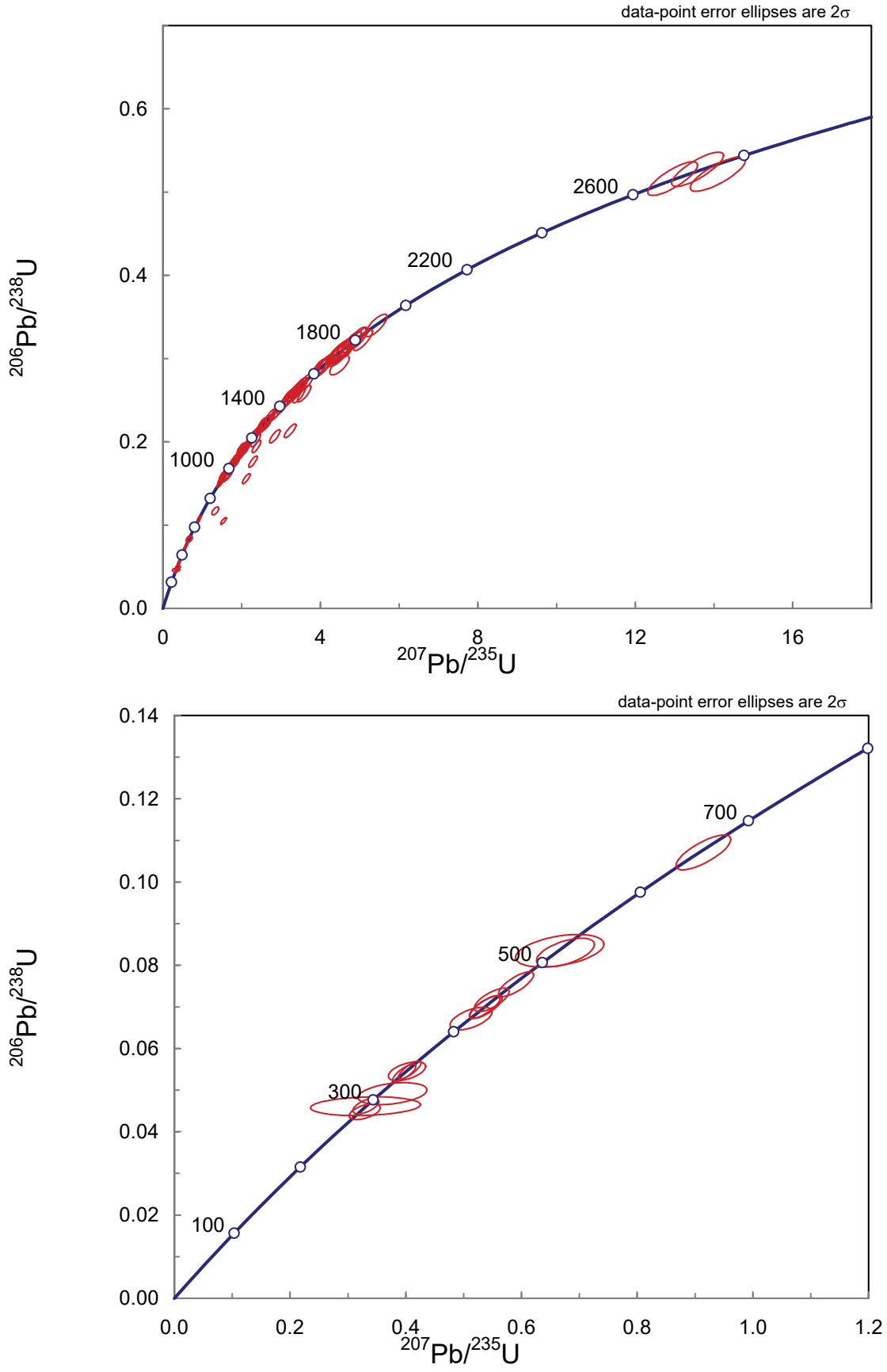

Fig. 7. U-Pb isotopic compositions of zircons from ditch cuttings sample at 9770-9820 ft in A15-01, displayed on Wetherill concordia diagrams. Upper shows all data, lower shows compositions of Phanerozoic and later Neoproterozoic grains. Note that the great majority of zircons display concordant or near-concordant compositions with error ellipses lying on the concordia line.

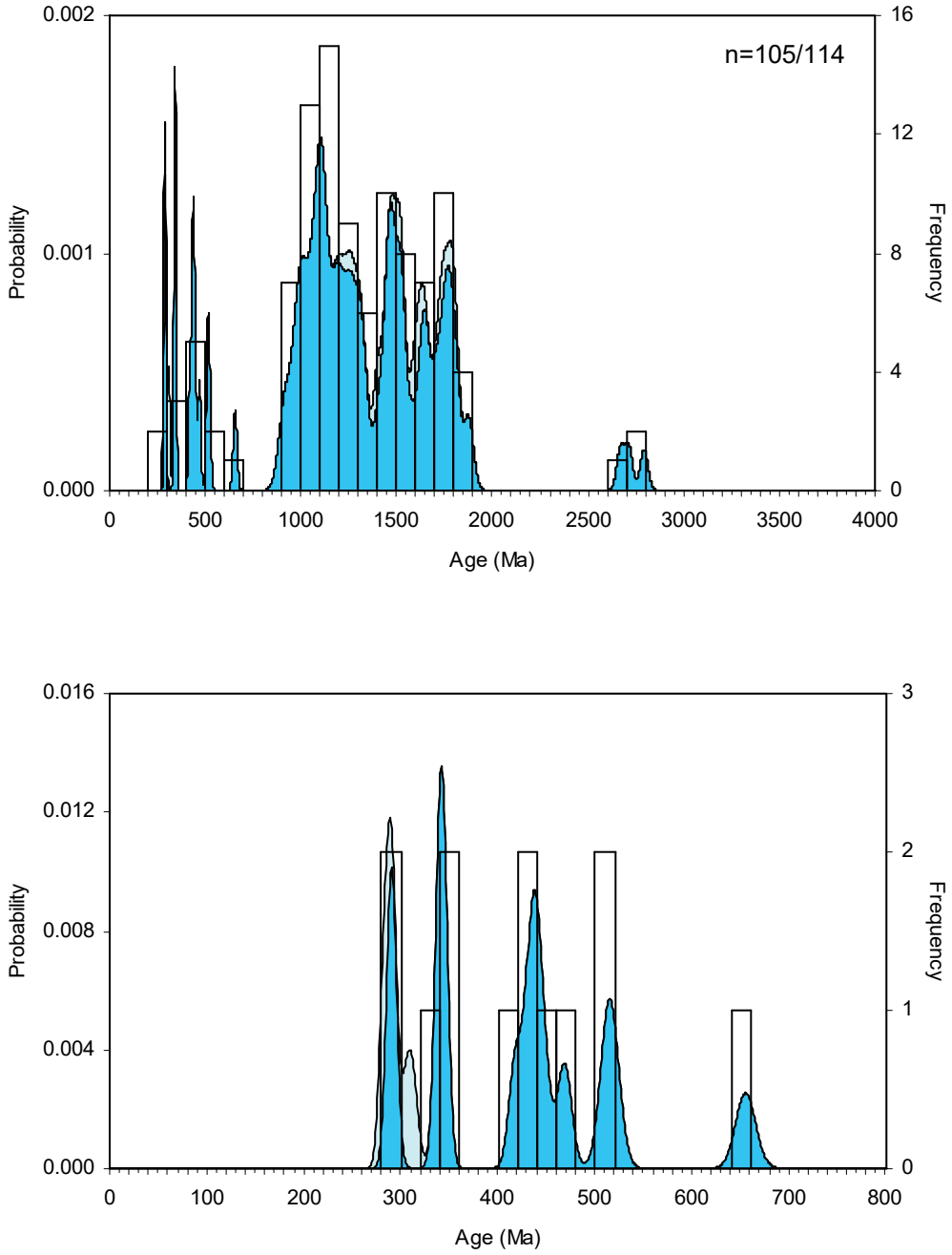

Fig. 8. Zircon age distribution in ditch cuttings sample from 9770-9820 ft in A15-01, displayed on probability-density plots. Upper shows entire spectrum, lower shows an expansion of the Phanerozoic and later Neoproterozoic. ‘n’ = number of analyses with < 10% discordance in the total zircon population

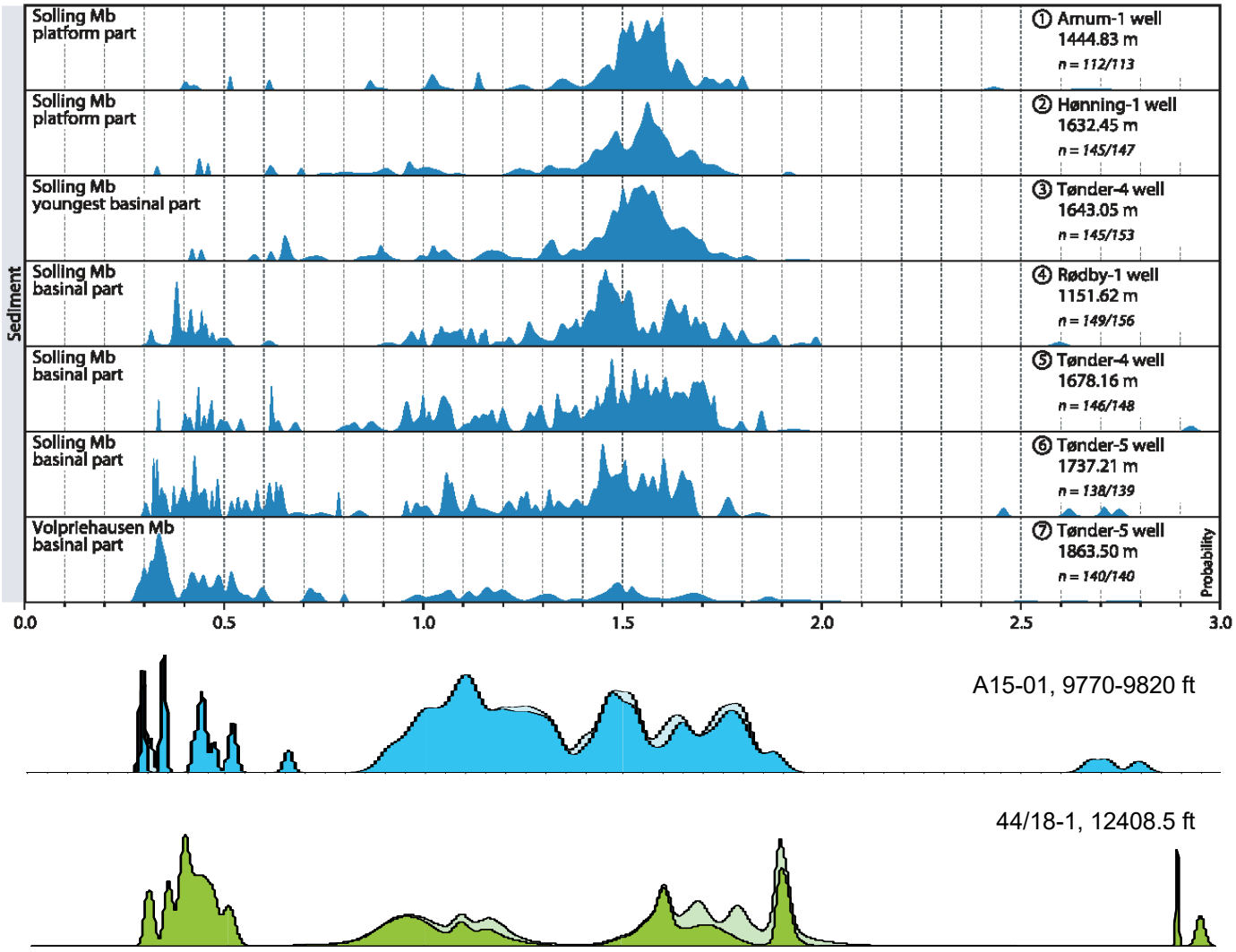

Fig. 9. Detrital zircon ages in Bunter sandstones from the North German Basin (Olivarius et al., 2015), compared with the analysed sample from A15-01. The North German Basin data show a shift from southerly-sourced to northerly-sourced sandstones between the Volpriehausen and Solling Members. The A15-01 sample has a small southerly component as seen in the Volpriehausen Mbr and older parts of the Solling Mbr, but differs from all North German Basin samples in having a large group of zircons with Sveconorwegian (900-1300 Ma) affinity. Also shown is the zircon spectrum from the Late Carboniferous Ketch Formation in the UK Southern North Sea, interpreted as having a source on the Ringkøbing-Fyn High (Morton et al., 2001; Morton et al., 2005).

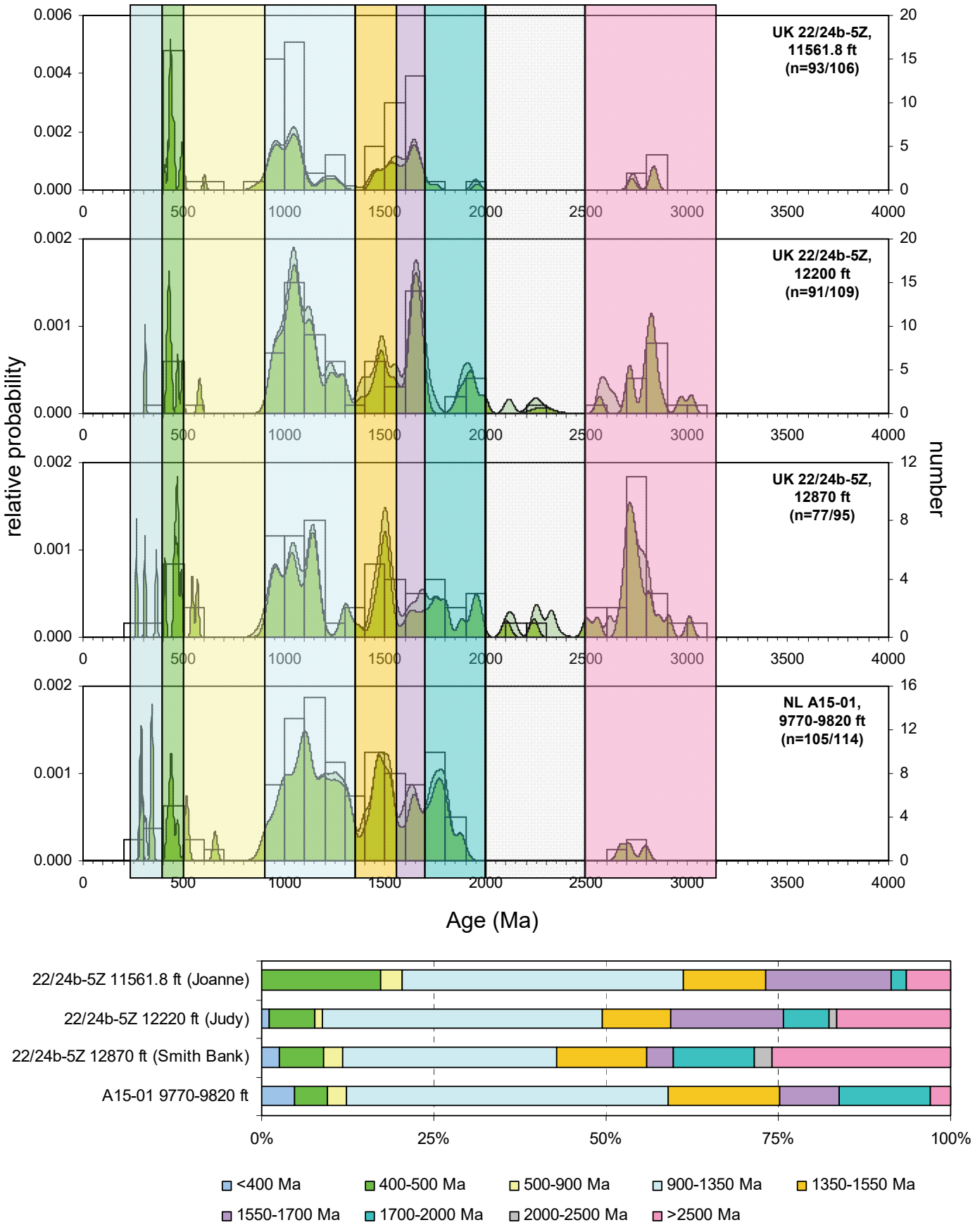

Fig. 10. Zircon ages in A15-01 compared with Smith Bank, Judy and Joanne sandstones from Marnock Field well UK 22/24b-5Z, and bar chart summarising differences in relative abundances of the main peaks. Marnock zircon data are from Greig (2021).